ChemCatChem

Supporting Information

# Efficient Oxygen Evolution Electrocatalyst by Incorporation of Nickel into Nanoscale Dicobalt Boride

Jona Schuch[+],* Sebastian Klemenz[+], Patrick Schuldt, Anne-Marie Zieschang, Stephanie Dolique, Paula Connor, Bernhard Kaiser, Ulrike I. Kramm, Barbara Albert, and Wolfram Jaegermann

# X-ray diffraction investigations

The software TOPAS V4.2 (Bruker AXS) was used for Rietveld profile analysis to determine the lattice parameters for $(Co_{1-x}Ni_x)_2B$ with $0 \leq x \leq 0.5$. The peak profile functions used were modified Thomson-Cox-Hastings pseudo-Voigt functions and Chebychev polynomials of an order of ten was used to fit the background. **Figure S1** shows the diffraction pattern for $(Co_{1-x}Ni_x)_2B$ phases after annealing at 500 °C. The refinement data for the samples is given in Table S1.

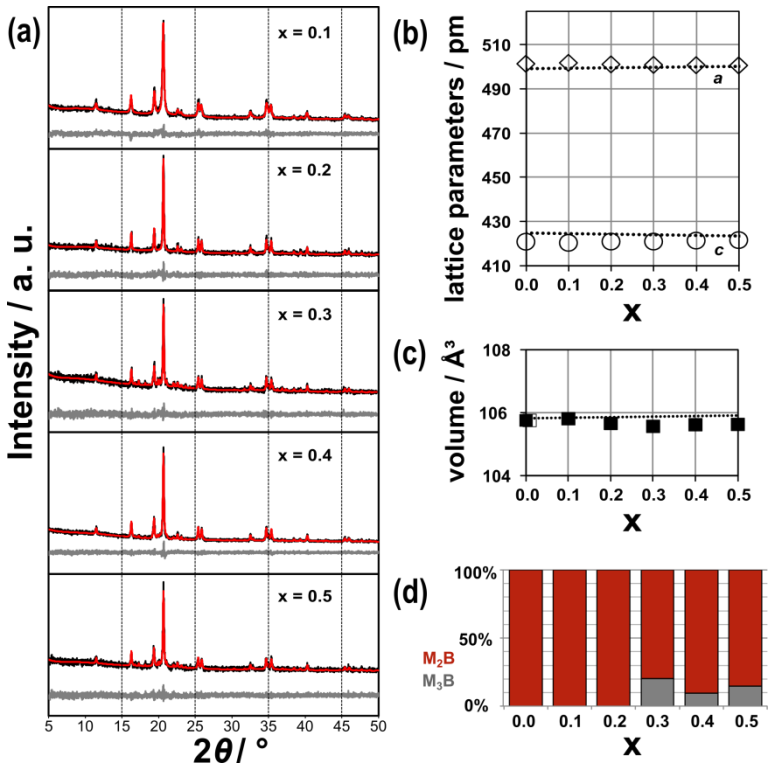


**Figure S1: (a)** XRD patterns of annealed $(Co_{1-x}Ni_x)_2B$ samples with $0 \leq x \leq 0.5$ and the lattice parameters **(b)** and cell volume **(c)** as well as the crystalline phase composition **(d)** for these samples determined using Rietveld analysis. The dotted line in **(b)** and **(c)** are supposed to lead the eye using Vegard's law.

**Table S1**: Rietveld refinement data for $(Co_{1-x}Ni_x)_2B$ and $Co_2B$ from [1].

| | **x = 0.0 Ref [1]** | **x = 0.1** | **x = 0.2** | **x = 0.3** | **x = 0.4** | **x = 0.5** |
|---|---|---|---|---|---|---|
| | **$(Co_{1-x}Ni_x)_2B$ *I4/mcm*; Z = 4** | | | | | |
| **Lattice parameters/ pm** | a = 501.33(3)<br>c = 420.84(4) | a = 501.76(3)<br>c = 420.33(4) | a = 501.06(3)<br>c = 420.91(4) | a = 500.84(3)<br>c = 420.91(4) | a = 500.71(2)<br>c = 421.34(3) | a = 500.60(4)<br>c = 421.56(5) |
| **Unit cell volume / Å³** | 105.77(2) | 105.82(2) | 105.67(2) | 105.58(2) | 105.63(1) | 105.64(2) |
| **Crystallite size (Lorentzian)** | 20.1(2) nm | 19.8(2) nm | 36.7(7) nm | 53(2) nm | 38.9(5) nm | 28.6(6) nm |
| **Linear absorption coefficient / $cm^{-1}$** | 334.52(4) | 334.34(5) | 334.81(4) | 335.11(5) | 334.94(4) | 334.91(6) |
| **Phase contribution** | 100% | 100% | 100% | 79.6(6) % | 90.6(4) % | 85.4(7) % |
| **$R_{Bragg}$** | 2,491 | 2,306 | 1,968 | 2,537 | 1,555 | 1,896 |
| | **$Ni_3B$ *Pbnm*; Z = 4** | | | | | |
| **Lattice parameters/ pm** | - | | | a = 439.48(7)<br>b = 522.39(9)<br>c = 661.7(2) | a = 439.0(3)<br>b = 522.9(4)<br>c = 662.6(5) | a = 439.2(1)<br>b = 522.3(2)<br>c = 662.6(3) |
| **Unit cell volume / Å³** | - | | | 151.91(5) | 152.1(2) | 151.75(8) |
| **Crystallite size (Lorentzian)** | - | | | 44(4) nm | 45(6) nm | 34(4) nm |
| **Linear absorption coefficient / $cm^{-1}$** | - | | | 397.9(2) | 397.4(5) | 398.3(3) |
| **Phase contribution** | - | | | 20.4(6) % | 9.4(4) % | 14.7(7) % |
| **$R_{Bragg}$** | - | | | 2.849 | 2.111 | 2.129 |
| **Temperature** | 293(2) K | 293(2) K | 293(2) K | 293(2) K | 293(2) K | 293(2) K |
| **Zero point error / 2θ** | 0.0000(7) ° | 0.015(3) ° | 0.0000(8) ° | 0.0015(8) | 0.0012(6) ° | 0.0001(9) ° |
| **Wavelength / Å** | 0.70930 Å | 0.70930 Å | 0.70930 Å | 0.70930 Å | 0.70930 Å | 0.70930 Å |
| **Range / 2θ** | 5-50 ° | 5-50 ° | 5-50 ° | 5-50 ° | 5-50 ° | 5-50 ° |
| **Rwp** | 7.56 | 7.75 | 12.75 | 12.13 | 8.83 | 13.83 |
| **Rp** | 5.97 | 6.05 | 9.91 | 9.28 | 6.95 | 10.63 |
| **GOF** | 1.03 | 1.01 | 0.95 | 0.94 | 0.95 | 0.91 |
| **Rexp** | 7.36 | 7.68 | 13.37 | 12.95 | 9.25 | 15.12 |

## Surface Analysis

The catalysts' bulk compositions were estimated by the used synthesis parameters and by an XRD analysis. The nickel to cobalt ratio was estimated from the amounts of the starting materials, cobalt(II) chloride hexahydrate (97 %, VWR) and nickel(II) chloride hexahydrate (98 %, Riedel-de Haën). The metal to boron ratio was calculated using the phase composition illustrated in **Figure S1d**, which was obtained from a Rietveld analysis of the XRD data of the catalyst powders.

The quantitative surface analysis was conducted with XPS on the powders embedded in indium foil. A Shirley background[2]was used for the XP detail spectra of the Co 2p, Ni 2p, and B 1s photoemission lines. The sensitivity factors were taken from [3]. The achieved phase compositions are illustrated in **Table S2**. The surface ratios of the $(Co_{1-x}Ni_x)_2B$ catalyst powders showed comparable nickel to cobalt ratios as expected from the synthesis. However, the $(Co_{1-x}Ni_x)_2B$ catalyst powders showed lower boron to metal ratios (0.38 to 0.35) than expected for $M_2B$ phases (0.5). This discrepancy can be explained by the formation of an $M_3B$ phase for $(Co_{1-x}Ni_x)_2B$ with $x \geq 0.3$ (**Figure S1d**) and by the visible surface oxidation revealed by XPS (**Figure 2**) and discussed in the main article.

**Table S2:** Bulk (synthesis) and surface (XPS) composition of $(Co_{1-x}Ni_x)_2B$ before the electrochemical investigation, calculated using a Shirley background [2] with sensitivity factors taken from [3].

| | **Bulk ratios (synthesis)** | | **Surface ratios (XPS)** | |
|---|---|---|---|---|
| **Sample** | Ni / Co | B / M | Ni / Co | B / M |
| **$(Co_{0.9}Ni_{0.1})_2B$** | 0.10 | 0.50 | 0.16 | 0.42 |
| **$(Co_{0.8}Ni_{0.2})_2B$** | 0.20 | 0.50 | 0.27 | 0.45 |
| **$(Co_{0.7}Ni_{0.3})_2B$** | 0.30 | 0.45 | 0.34 | 0.43 |
| **$(Co_{0.6}Ni_{0.4})_2B$** | 0.40 | 0.48 | 0.44 | 0.38 |
| **$(Co_{0.5}Ni_{0.5})_2B$** | 0.50 | 0.47 | 0.51 | 0.40 |

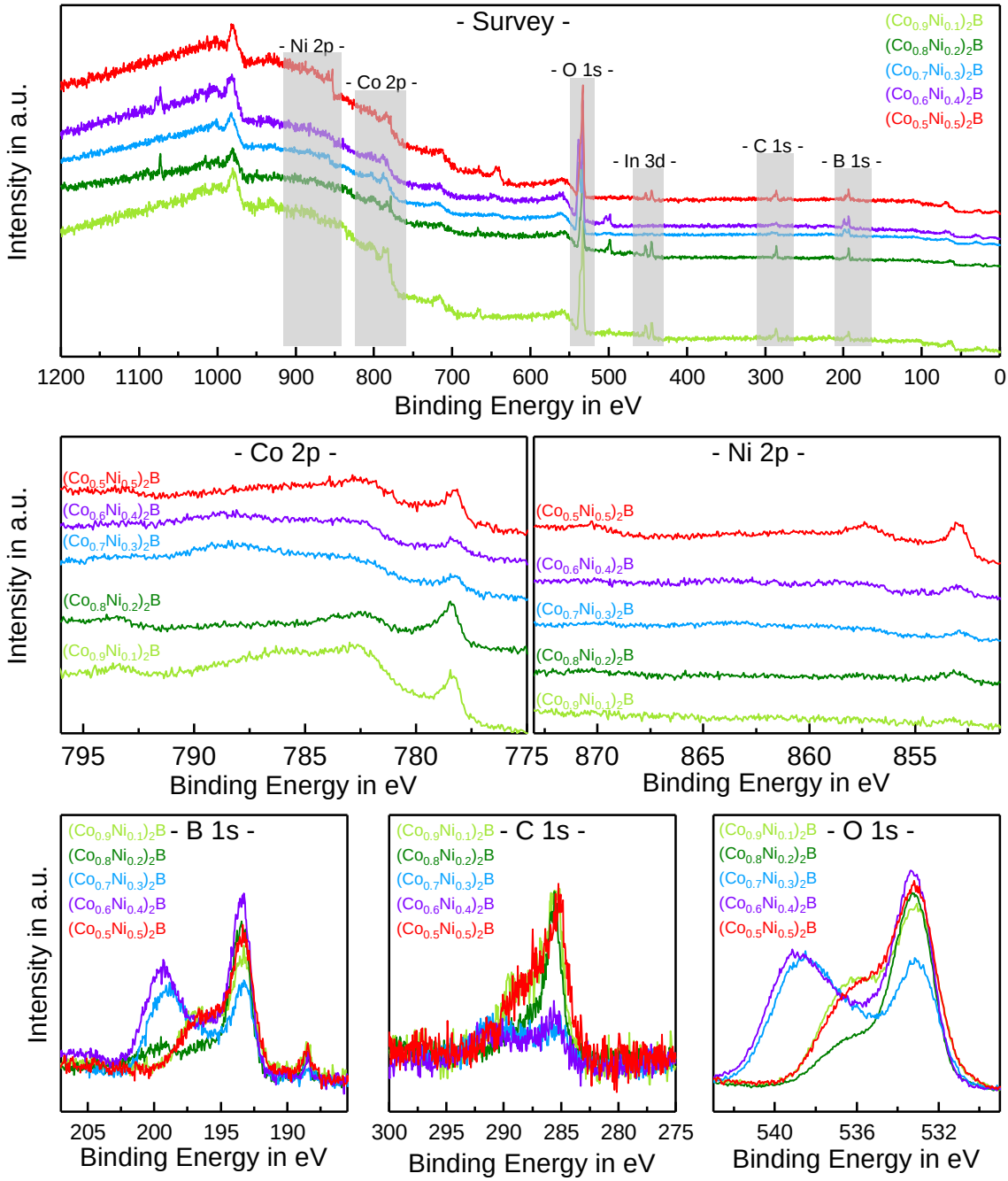


**Figure S4:** XPS survey, Co 2p, Ni 2p, B 1s, C 1s, and O 1s photoemission lines of $(Co_{1-x}Ni_x)_2B$ with $0 \leq x \leq 0.5$ embedded in indium foil before the electrochemical investigation.

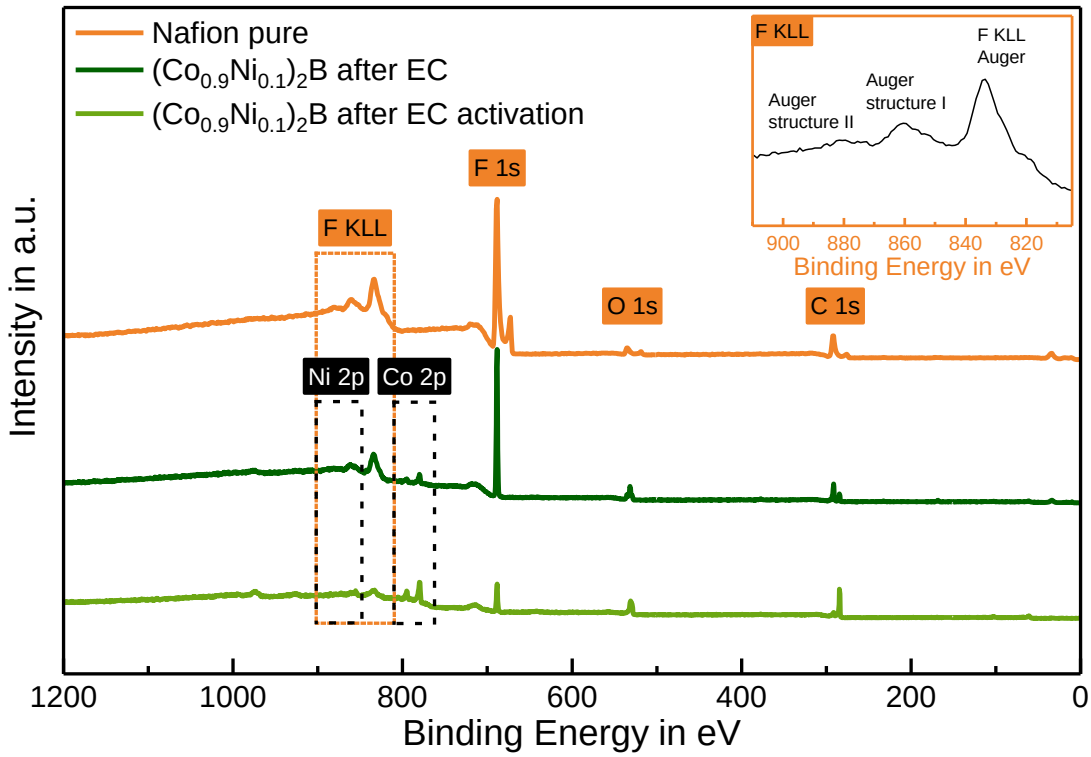


**Figure S5:** XP survey spectra of Nafion® and $(Co_{0.9}Ni_{0.1})_2B$ drop coated in a Nafion® containing ink after EC activation and after EC. The inset illustrates the structure of the fluorine F KLL Auger.

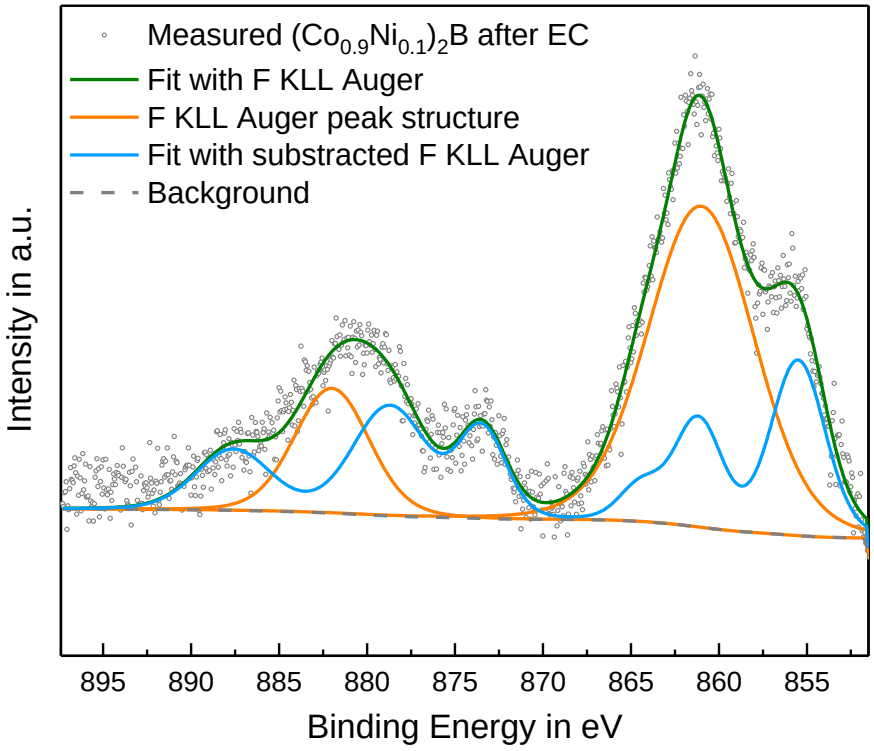


**Figure S6:** Measured Ni 2p XPS photoemission line of the with Nafion® drop coated $(Co_{0.9}Ni_{0.1})_2B$ catalyst after the electrochemical testing (black dotted). The fitted F KLL Auger

peak structure is marked in orange, which was subtracted from the measured signal (dark green), resulting in the pure Ni 2p photoemission line of the catalyst (light blue).

# Electrochemical Investigations

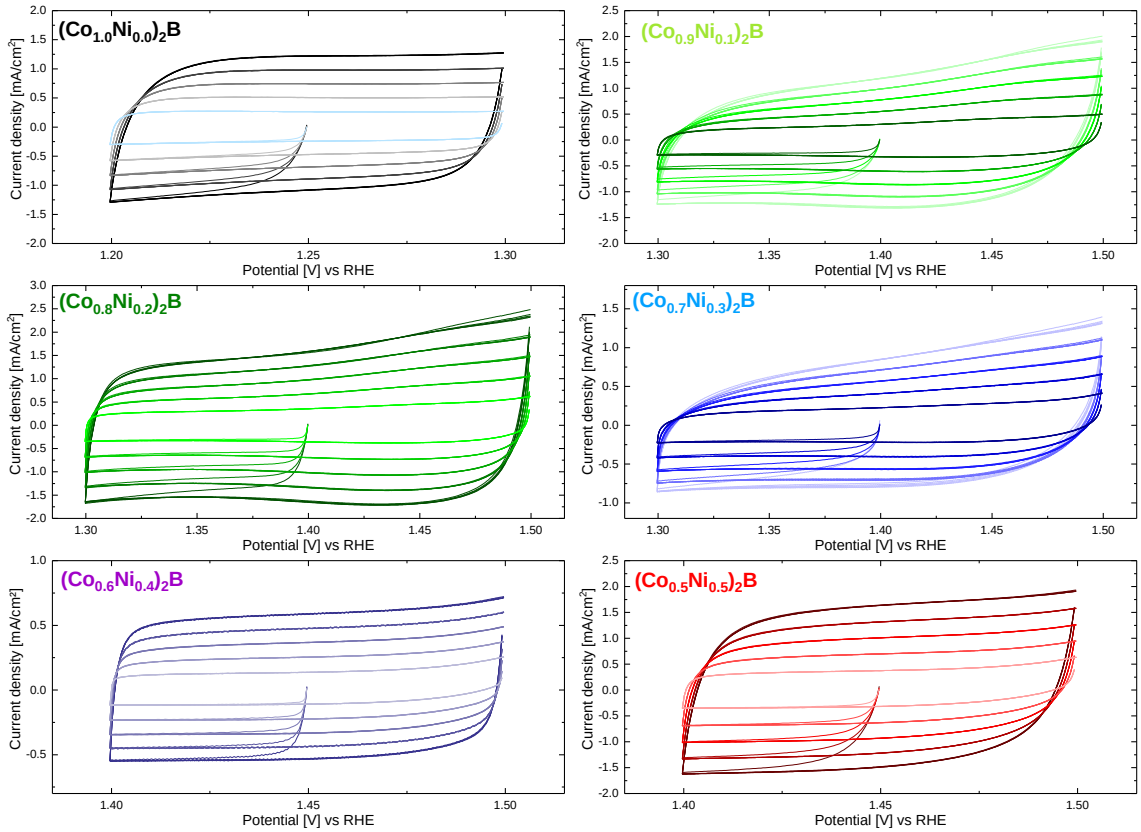


**Figure S7:** Potential sweep curve measurements between 1.2 and 1.5 V vs. RHE for $(Co_{1-x}Ni_x)_2B$ with $0 \leq x \leq 0.5$. The measurement for pure $Co_2B$ (black) was measured at slightly lower potentials due to an overlap with a redox wave. The cyclic voltammograms are measured at a scan rate of 10, 20, 30, 40, and 50 mV $s^{-1}$.

**Table S3:** OER overpotential comparison values of other mixed-metal-boride based catalyst system in alkaline electrolyte with the corresponding references, used substrates and catalyst loadings. (Overpotential was measured at beginning of test (BoT) and end of test (EoT) with an eight hour GSS in-between)

| Catalyst | Substrate | Electrolyte | Loading mg $cm^{-2}$ | OER Overpotential in mV @ 10 mA $cm^{-2}$ | Reference |
|---|---|---|---|---|---|
| $(Co_{0.9}Ni_{0.1})_2B$ | GC | 1 M KOH | 0.150 | 371 (BoT)<br>355 (EoT) | This work |
| $Co_{0.9}$-$Ni_{0.1}$-B | GC | 1 M KOH | 0.294 | 330 | [4] |
| Co-2.3Ni-B | GC | 1 M KOH | 0.300 | 317 | [5] |
| $Co_{0.96}$-$Ni_{0.04}$-$B_3$ | Ni foam | 1 M KOH | - | 313 | [6] |
| $(Co_{0.7}Fe_{0.3})_2B$ | GC | 1 M KOH | 0.150 | 330 | [1] |
| Co2-Fe-B | Cu | 1 M KOH | 1.200 | 298 | [7] |
| $Co_{0.7}Fe_{0.3}$-B | GC | 1 M KOH | 0.300 | 282 | [8] |
| Fe-2.3Ni-B | GC | 1 M KOH | 0.300 | 294 | [5] |
| Ni-Fe-B | GC | 1 M KOH | 0.200 | 340 | [9] |
| Fe-Co-2.3Ni | GC | 1 M KOH | 0.300 | 274 | [5] |

## Transmission electron microscopy

TEM and STEM images of the catalyst show a layer of low contrast material encasing a crystalline core (**Figure S8a,b**). The electron diffraction pattern (**Figure S8c,d**) was compared to a simulated pattern based on the lattice parameters derived from XRD data (**Table S1**) of $(Co_{0.9}Ni_{0.1})_2B$. The result is in agreement to the XRD data and implies the surface layer around the particles to be amorphous. Using STEM (**Figure S8e,f**) the chemical composition of the catalyst was analyzed using EDX. The particles consist of cobalt, nickel and oxygen with impurities of carbon and silicon. Due to instrumental limitation, the detection of boron was not possible. EDX-mapping (**Figure S8g**) shows the layer to be oxygen-rich, confirming the XPS data interpretation (**Figure 2**), and the analysis of line profiles (**Figure S8h**) is in tune with an oxygen-rich surface layer. However, at this stage the material does not have a metal oxide layer as shown by the different on-sets of the oxygen and metal intensities in the EDX

line profile. XPS data provides evidence for a boron oxide layer covering the surface (**Figure 2b**), which explains the missing signals from cobalt and nickel at the particles surface.

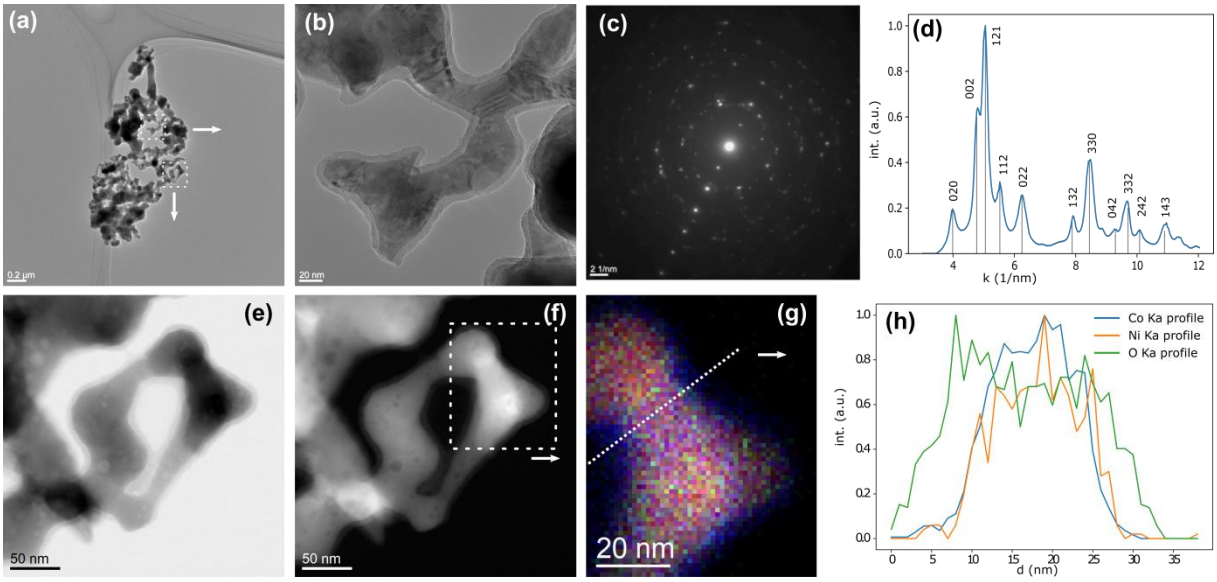


**Figure S8:** TEM images (a,b), selected area electron diffraction (SAED) pattern (c), bright-field (BF) STEM image (e), high-angle annular dark-field (HAADF) image (f), and EDX map of catalyst before making the ink. (d) Shows the rotational average of the SAED pattern of the catalyst with simulated Bragg peak positions for the $(Co,Ni)_2B$ phase and (h) $K_\alpha$ line profiles of the EDS data including Co (blue), Ni (orange), and O (green).

**References**


[1] S. Klemenz, J. Schuch, S. Hawel, A. M. Zieschang, B. Kaiser, W. Jaegermann, B. Albert, *ChemSusChem* **2018**, *11*, 3150.

[2] D. A. Shirley, *Phys. Rev. B* **1972**, *5*, 4709.

[3] J. H. Scofield, *J. Electron Spectros. Relat. Phenomena* **1976**, *8*, 129.

[4] J. Zhang, X. Li, Y. Liu, Z. Zeng, X. Cheng, Y. Wang, W. Tu, M. Pan, *Nanoscale* **2018**, *10*, 11997.

[5] J. M. V. Nsanzimana, Y. Peng, Y. Y. Xu, L. Thia, C. Wang, B. Y. Xia, X. Wang, *Adv. Energy Mater.* **2018**, *8*, 1.

[6] N. Xu, G. Cao, Z. Chen, Q. Kang, H. Dai, P. Wang, *J. Mater. Chem. A* **2017**, *5*, 12379.

[7] H. Chen, S. Ouyang, M. Zhao, Y. Li, J. Ye, *ACS Appl. Mater. Interfaces* **2017**, *9*, 40333.

[8] J. M. V. Nsanzimana, L. Gong, R. Dangol, V. Reddu, V. Jose, B. Y. Xia, Q. Yan, J. M. Lee, X. Wang, *Adv. Energy Mater.* **2019**, *1901503*, 1.

[9] L. An, Y. Sun, Y. Zong, Q. Liu, J. Guo, X. Zhang, *J. Solid State Chem.* **2018**, *265*, 135.